
EXAMINING THE MAPPING FUNCTIONS OF DENOISING AUTOENCODERS IN MUSIC SOURCE SEPARATION

Stylianos Ioannis Mimilakis*

Fraunhofer-IDMT
Ilmenau, Germany

Konstantinos Drossos

Audio Research Group
Tampere University
Tampere, Finland

Estefanía Cano

Fraunhofer-IDMT
Ilmenau, Germany

Gerald Schuller

Dpt. for Media Technology
Technical University of Ilmenau
Ilmenau, Germany

ABSTRACT

The goal of this work is to investigate what music source separation approaches based on neural networks learn from the data. We examine the mapping functions of neural networks that are based on the denoising autoencoder (DAE) model, and conditioned on the mixture magnitude spectra. For approximating the mapping functions, we propose an algorithm that is inspired by the knowledge distillation and is denoted as the neural couplings algorithm (NCA). The NCA yields a matrix that expresses the mapping of the mixture to the target source magnitude information. Using the NCA we examine the mapping functions of three fundamental DAE models in music source separation; one with single layer encoder and decoder, one with multi-layer encoder and single layer decoder, and one using the skip-filtering connections (SF) with a single encoding and decoding layer. We first train these models with realistic data to estimate the singing voice magnitude spectra from the corresponding mixture. We then use the optimized models and test spectral data as input to the NCA. Our experimental findings show that approaches based on the DAE model learn scalar filtering operators, exhibiting a predominant diagonal structure in their corresponding mapping functions, limiting the exploitation of inter-frequency structure of music data. In contrast, skip-filtering connections are shown to assist the DAE model in learning filtering operators that exploit richer inter-frequency structure.

Keywords Music source separation, denoising autoencoder, DAE, skip connections, neural couplings algorithm, NCA

1 Introduction

Signal enhancement and separation based on deep learning methods is an active research area that has attracted a lot of attention [1]. The objective is to estimate an individual target signal from an observed corrupted version. In the context of music source separation, the corrupted observation refers to the observed mixture signal and the individual target signal to the isolated music source, e.g. singing voice, drums, etc. A particularly challenging task in music source separation is the estimation of singing voice from a single channel, i.e., *monaural*, mixture signal [2]. To that aim, deep learning approaches are shown to yield state-of-the-art (SOTA) results [3].

The majority of deep learning approaches use the time-frequency representation of the mixture signal as input [3, 2]. However, based on the target output signal we can identify three different classes of approaches. The approaches in the first class use as a target output the time-frequency representation of the target source, following the seminal work of the DAE model that is presented in [4, 5]. In the second class of approaches, the target signal is explicitly the pre-computed and source dependent time-varying filter, i.e., the *mask*, that is used for filtering the mixture input signal [6, 7, 8]. The usage of pre-computed masks imposes various assumptions regarding the additive properties of the sources [9, 10]. This has led to research advocating the need for masks to be subject to optimization [11]. The approaches in the third class combine the two previous classes. Specifically, these methods allow deep learning based approaches to implicitly mask the input mixture signal by using the output of the deep learning model [12, 13, 14, 15]. This operation yields a

*Corresponding author: mis@idmt.fraunhofer.de

filtered version of the mixture signal that serves as an estimate of the target source signal, and is used to optimize the overall approach [12, 14, 15]. Approaches falling into the third class are commonly denoted as the signal approximation method and/or as the *skip-filtering connections*, in the context of speech enhancement and separation [12, 16] and music source separation [14, 17, 18], respectively.

The approaches in the first class rely on a post-processing step based on the generalized Wiener filtering, in order to estimate the target source signal(s) [19, 20, 21, 22, 6, 2, 17, 3]. The post-processing is an empirical requirement for obtaining target signals of better, than the direct outputs of the DAEs, quality [19, 20]. In contrast, approaches in the third class, which employ the implicit masking of the mixture signal, yield competitive results compared to the first class of approaches without the necessity of post-processing steps [18, 15]. Furthermore, approaches in the third class outperform approaches in the second class that explicitly predict the corresponding masks [14, 17]. In relevant literature, for instance the big scale study presented in [3], it is not clear why approaches that focus on target source signal prediction [19, 22, 21] require the post-processing step of generalized Wiener filtering. It is also intriguing to provide an explanation on why predicting time-frequency masks, either explicitly [6, 7] or implicitly [17, 12, 15], works well in practice. With this in mind, we formulate the first research question of our work: ***RQ1 - Why is masking important in approaches based on the DAE model?***

Additionally, the work presented in [23] underlines the tendency of the encoding and decoding functions of the DAE to become symmetric during training. The composition of symmetric functions yields another function, used to map the input to the target signal, i.e., the *mapping function*, that shares many similarities with the identity function. For spectral-based denoising, that could potentially result into poor estimation of the target source spectra, unless the learned function is derived from an ideal and time-variant frequency mask [24], computed using an appropriate time-frequency masking technique [25]. Subsequently, the second research question of our work is: ***RQ2 - Do DAEs that are commonly employed in music source separation learn trivial solutions for the given problem?***

In this study, we try to answer the above research questions by examining the mapping functions of music source separation approaches that have been proposed to estimate the target source magnitude spectra. Considering that our general goal is to get insights about what data-driven approaches have learned to this specific problem, standard source separation evaluation criteria such as the signal-to-distortion ratio fall short. Since nearly all music separation approaches are non-linear, the computation of the mapping function is not straightforward. To tackle that, we propose an experimentally derived algorithm that approximates the mapping function of the non-linear model previously optimized for source separation. The result of the algorithm is a matrix that is utilized to linearly map the magnitude information of the mixture to the target source magnitude spectra. We will henceforth denote the algorithm as the *neural couplings algorithm* (NCA).

The goal of the NCA is to compute a linear mapping function that describes how the input data are transformed to obtain the desired target source, according to the approach under examination. The NCA differs from methods that aim at explaining the neural network decisions, like for instance the layer-wise relevance propagation method presented in [26], but shares many similarities with the optimal transportation theory, in the discrete case [27, 28], and the knowledge distillation concept presented in [29]. The conceptual difference between the NCA and the previously stated methods is that the NCA specifically approximates the mapping function of a pre-trained neural network model. It does not aim at compressing the neural network model as in [29], or computing only distance dependent mapping(s) between spectral data distributions as in [28], or at pin-pointing input spectral features that affect the choice of the neural network model as in [26].

In this study, we cluster the three previously described classes of deep learning-based music source separation approaches under the general class of DAEs, since they follow the same principles as the DAEs presented in [4, 5]. Specifically, we focus on three particular and fundamental extensions, i.e., models of the DAE that have been proposed for music source separation. In more details, we examine:

1. **DAE:** The DAE model presented in [4], as it forms the baseline that source separation approaches have built upon.
2. **MSS-DAE:** The multi-layered extension of the DAE following the pioneering works in [19, 22].
3. **SF:** The implicit mask prediction via the skip-filtering (SF) connections employed in [14, 12, 15].

In all three models we employ the rectified linear unit activation function (ReLU) as it was shown experimentally in [19] to perform well in music source separation tasks. The target signal to be estimated by each model is the singing voice spectra. For assessing the mapping functions of each model, we use the outcome of the NCA, and objectively compute a fraction of the magnitude contained in the main and off diagonal elements of the computed by the NCA matrix. This will be explained in details in the following sections.

The rest of this document is organized as follows: Section 2 provides background information on the DAEs and the variations proposed for the problem of music source separation tasks. Our proposed NCA algorithm is described in Section 3, followed by Section 4 that describes the experimental procedure. Our experimental findings are presented and discussed in Section 5. Section 6 concludes this work and underlines future research directions.

2 Denoising Autoencoders in Music Source Separation

2.1 Background

Music source separation based on DAEs relies on a supervised learning scenario. Formally, given a data-set $\mathcal{D} = \{\tilde{x}^{(i)}, x^{(i)}\}_{i=1}^K$, comprised of $K \in \mathbb{Z}^+$ training examples indexed by i , the goal is to learn a denoising function f . The function f is parameterized by θ , and estimates the clean x from the noisy \tilde{x} observation, i.e., $f : \theta \times \tilde{x} \mapsto x$. Obtaining \tilde{x} involves a mixing process, which for audio signals, is commonly assumed to be the addition of the interfering or noise signal x_n and the target source x signal [17], i.e., $\tilde{x} = x + x_n$. Given a reconstruction loss function \mathcal{L} , the parameters θ are optimized using

$$\theta^o = \underset{\theta}{\operatorname{argmin}} \sum_{i=1}^K \mathcal{L}(x^{(i)}, \hat{x}^{(i)}), \quad (1)$$

where \hat{x} is an estimate of x , and θ^o is the optimal parameter, or set of parameters, that minimize the cost. The updates of the parameters towards obtaining θ^o is carried out using stochastic gradient descent over samples drawn from the data-set \mathcal{D} .

In [4], two functions are introduced through the DAE structure in order to approximate f , namely $f_{\text{enc}} : \theta_{\text{enc}} \times \tilde{x} \mapsto z$ and $f_{\text{dec}} : \theta_{\text{dec}} \times z \mapsto x$. The parameters $\theta := \{\theta_{\text{enc}}, \theta_{\text{dec}}\}$ are optimized with respect to Eq. (1). In the context of music source separation, the motivation is to learn the empirical distribution $q(x|\tilde{x})$ through the usage of a latent representation z , and the utilization of the decoding process f_{dec} . The benefit of incorporating the latent variable z into the model is that it provides a feature space that is useful for denoising auto-encoding [4] and music source separation [19, 6, 22]. An illustration of the DAE model is given in Fig. 1.a.

In music source separation approaches, the computation of the latent variable z plays an important role [6, 20, 22, 19]. Specifically, the performance of the methods, and the approximation of the target source x is shown empirically [6, 22, 19] to be based on the computation of z_ℓ , a deeper hidden representations of z that leads to the conditional distribution $q(z_\ell|z_{\ell-1})$. The subscript $\ell \in \{1, 2, \dots, L\}$ denotes the depth of the computed, hidden representations. The corresponding graphical depiction of the a three layer example of the MSS-DAE is given in Fig. 1.b.

It is important to note that source separation approaches based on skip filtering connections, which implicitly predict the mask (i.e., approaches falling in the third class, mentioned in Section ??), use the same two functions as in the DAE, i.e., f_{enc} and f_{dec} . The difference is that $f_{\text{dec}} : \theta_{\text{dec}} \times z \mapsto m$, and

$$x = m \odot \tilde{x}, \quad (2)$$

where m is the mask and \odot is the Hadamard (element-wise) product. Eq. (2) is implemented by the skip connections which allow \tilde{x} to be propagated to both encoding and after the last decoding function of the model [14, 12, 16]. The SF models the empirical distribution $q(x|\tilde{x})$ using $q(m|\tilde{x})q(\tilde{x})$, as illustrated in Fig.1.c. Subject to the target source x , the aforementioned empirical distribution leads to $q(x|\tilde{x})q(\tilde{x})$ since both the mask m and the target signal x are computed as a function of \tilde{x} , i.e., $x = f_{\text{dec}}(f_{\text{enc}}(\tilde{x})) \odot \tilde{x}$. That differs from the DAE and MSS-DAE that model directly $q(x|\tilde{x})$. For the SF model and its corresponding conditional, the product between distributions is the element-wise product of the probability values between the outcome of the DAE and \tilde{x} .

2.2 Prior Work

The most widely adopted way to perform music source separation using deep learning is to employ the magnitude spectral representations computed using the short-time Fourier transform (STFT). This is performed in order to reduce the overlap that the sources exhibit in the time-domain signal representation [30], and to exploit the wide-sense stationarity and the phase-invariant structure(s) of specific types of music sources [31]. Therefore, we can think of the variables of the DAE, MSS-DAE, and SF models as vectors containing magnitude spectral information. Nonetheless, the additive properties of the mixing process for computing \tilde{x} do not hold, i.e., $\tilde{x} \neq x + x_n$ since the phase information has been discarded. More specifically, $\tilde{\mathbf{x}}, \hat{\mathbf{x}}, \mathbf{x} \in \mathbb{R}_{\geq 0}^N$, and $\mathbf{z} \in \mathbb{R}^F$ are the mixture signal, the estimated target source signal, the target source signal, and the latent representation after the application of the ReLU function, respectively. The N and F denote the dimensionality of the input and hidden representations, respectively.

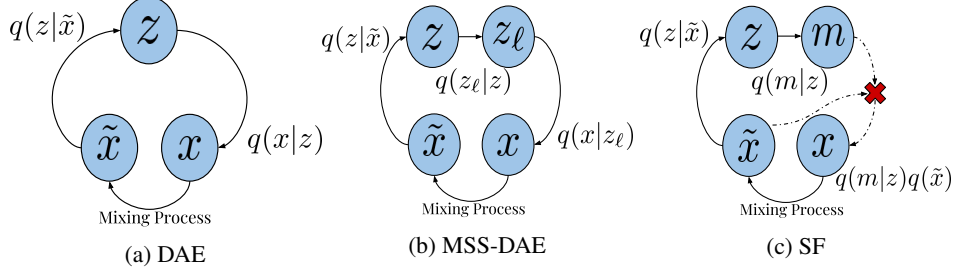


Figure 1: Illustration of the graphical models of encoder-decoder configurations examined in this work. (a) *DAE*: a denoising auto-encoder model [4]. (b) *MSS-DAE*: a three layer example of a DAE model adapted to music source separation [19, 22]. (c) *SF*: skip-filtering connections [14, 17, 12, 15]. Solid arrows are functions computed by neural networks. Dashed arrows are the identity function. The red “ \times ” refers to the Hadamard (element-wise) product.

For source estimation based on DAEs, the authors in [22] propose the use of multi-layered feed-forward neural networks, using context information of past and future STFT magnitude spectra. Aiming to model the dependencies of adjacent time-frames, the work in [20] proposes to use bi-directional RNNs instead of feed-forward neural networks. In both approaches [20, 22], the estimated target sources are refined by using multi-channel Wiener filtering [20], and a variant based on the expectation-maximization algorithm [22]. In contrast, the work presented in [6] proposes to explicitly predict pre-computed time-frequency masks using deep neural networks. After the mask prediction, the masks are applied to the mixture signal and then refine the estimates using DAEs. More robust approaches allow implicit mask prediction by introducing the time-frequency masking operation into the computational graphs [14, 17, 12, 13, 32, 15, 33] by incorporating the skip connections described in Section 2.1.

The skip connections are a straightforward extension of the denoising source separation (DSS) framework in the spectral domain presented in [24]. In the DSS framework, it is proposed to perform spectral-based denoising by learning a sparse matrix with non-zero elements only on the main diagonal. These elements allow a scalar filtering operation [34] of each corresponding frequency sub-band. In music source separation works based on deep learning, the previously mentioned frequency sub-band scaling is achieved by employing the Hadamard product. That enables the usage of architectures that encompass time varying information, such as RNNs and/or CNNs, and therefore the prediction of time varying frequency masks. More specifically, the work in [13] proposes to employ deep RNNs for estimating the magnitude of all the sources contained in the mixed signal. The output estimates are then given to a deterministic function which yields source-dependent time-frequency masks by computing the ratio of the estimates. In this approach, RNNs do not learn the masking process, but rather to output magnitude estimates of the source that can be used to compute the mask. Aiming to also learn the masking process, i.e., allow the neural network to generate mask estimates without the necessity of devising rational models like in [13], the skip-filtering connections were introduced in [14], where an RNN encoder-decoder is responsible for the generation of a mask that estimates the singing voice. Extensions that improve the mask generation process of the model presented in [14] are discussed in [17, 18]. An alternative architecture is presented in [15], where ladder-like structured CNNs are proposed for singing voice separation via the aforementioned mask generation process.

2.3 Implementing the Models

Focusing on the graphical models presented in Figure 1, we constrain the problem to fully-connected, feed-forward neural network (FNN) layers, and to the minimization of the mean squared error (MSE) loss function, defined as:

$$\mathcal{L}_{\text{MSE}}(\mathbf{x}^{(i)}, \hat{\mathbf{x}}^{(i)}) = \frac{1}{N} \|\mathbf{x}^{(i)} - \hat{\mathbf{x}}^{(i)}\|_2^2, \quad (3)$$

where $\|\cdot\|_2$ denotes the ℓ_2 vector norm.

Stochastic gradient descent is performed to optimize the model parameters with respect to Eq. (3). This training configuration including the MSE was adopted from SOTA approaches in music source separation [21, 20, 14, 22, 19, 35]. An example of the calculation of z and the approximation of the i -th data example of the source $\hat{\mathbf{x}}$, using the mixture signal $\tilde{\mathbf{x}}$ and the corresponding encoding and decoding functions is given in Eqs. (4)–(10) for the DAE, MSS-DAE, and

SF models.

$$\mathbf{z}_{\text{DAE}}^{(i)} = g(\mathbf{W}_{\text{enc}} \tilde{\mathbf{x}}^{(i)} + \mathbf{b}_{\text{enc}}), \quad (4)$$

$$\hat{\mathbf{x}}_{\text{DAE}}^{(i)} = g(\mathbf{W}_{\text{dec}} \mathbf{z}_{\text{DAE}}^{(i)} + \mathbf{b}_{\text{dec}}), \quad (5)$$

$$\mathbf{z}_{\text{MSS-DAE}}^{(i)} = g(\mathbf{W}^{(\ell=1)} g(\mathbf{W}_{\text{enc}} \tilde{\mathbf{x}}^{(i)} + \mathbf{b}_{\text{enc}}) + \mathbf{b}^{(\ell=1)}), \quad (6)$$

$$\hat{\mathbf{x}}_{\text{MSS-DAE}}^{(i)} = g(\mathbf{W}'_{\text{dec}} \mathbf{z}_{\text{MSS-DAE}}^{(i)} + \mathbf{b}'_{\text{dec}}), \quad (7)$$

$$\mathbf{z}_{\text{SF}}^{(i)} = g(\mathbf{W}''_{\text{enc}} \tilde{\mathbf{x}}^{(i)} + \mathbf{b}''_{\text{enc}}), \quad (8)$$

$$\hat{\mathbf{x}}_{\text{SF}}^{(i)} = g(\mathbf{W}''_{\text{dec}} \mathbf{z}_{\text{SF}}^{(i)} + \mathbf{b}''_{\text{dec}}) \odot \tilde{\mathbf{x}}^{(i)}, \text{ where} \quad (9)$$

$$g(x) = \max(0, x). \quad (10)$$

Eqs. (4), (6), and (8) describe the encoding functions, and Eqs. (5), (7), and (9) the decoding functions of each model. The weight matrices and bias terms are denoted by \mathbf{W} and \mathbf{b} , respectively, and the subscripts “enc” and “dec” stand for encoder and decoder layers, respectively. The superscripts “/” and “//” in the weights and biases are used to distinguish between the parameters of different models (e.g. between \mathbf{W} of MSS-DAE and DAE models). In more detail, Eqs. (4) and (5) express the encoding and decoding functions for the DAE model. The process of approximating the source through the decoding function of a three layer example of the MSS-DAE model is given in Eqs. (6) and (7). The SF model in Eqs. (8) and (9) employs the same encoding and decoding configuration as the DAE, with the only difference the output of the decoding is element-wise multiplied with the input to the model. In the Eqs. (4)–(9) the encoding and decoding functions are realized as linear operators (i.e., vector-matrix product) that are then followed by the ReLU activation function expressed in Eq. (10).

3 Neural Couplings Algorithm

The NCA is an iterative method for approximating the mapping function of a non-linear source separation model. The mapping function is an affine transformation of magnitude spectral data. We constrain the affine transformation to be linear and model dependent in order to allow us to intuitively examine what each source separation model has learned. That affine transformation is represented by a matrix that we denote as the *couplings matrix* $\mathbf{C} \in \mathbb{R}^{N \times N}$. The couplings matrix \mathbf{C} is used to transform/map the input mixture magnitude spectrum $\tilde{\mathbf{x}}$ to the output $\mathbf{y} \in \mathbb{R}_{\geq 0}^N$ of the last layer of each corresponding model, i.e., the output of the decoding matrix followed by the ReLU function. The indexing by i in $\tilde{\mathbf{x}}$ and \mathbf{y} is dropped in order to denote the usage of spectral data that are not sampled from the training data-set. The vector \mathbf{y} is used to denote the output of the decoding function in each model. That output for the DAE and MSS-DAE models is the singing voice spectra $\hat{\mathbf{x}}$, and for the SF model is the derived frequency mask.

In the ideal case that each model is linear, the couplings matrix, and thus the mapping function, is expressed algebraically as the product of the corresponding encoding and decoding matrices. We denote that product as the *linear composition*. The linear composition, neglecting the bias terms for brevity in the notation, is computed for each model using:

$$\mathbf{C}_{\text{linear-DAE}}^o = \mathbf{W}_{\text{dec}} \mathbf{W}_{\text{enc}}, \quad (11)$$

$$\mathbf{C}_{\text{linear-MSS-DAE}}^o = \mathbf{W}'_{\text{dec}} \mathbf{W}^{(\ell=1)} \mathbf{W}'_{\text{enc}}, \text{ and} \quad (12)$$

$$\mathbf{C}_{\text{linear-SF}}^o = \mathbf{W}''_{\text{dec}} \mathbf{W}''_{\text{enc}}. \quad (13)$$

As the DAE, MSS-DAE, and SF, models are non-linear, employing directly Eqs. (11)–(13) would result into rather crude approximations of the models’ mapping functions. Even the linear behaviour of the ReLU function in the non-negative range, and of the vector-matrix products expressed in Eqs. (4)–(9), is not sufficient for the above linear composition functions to hold. The ReLU function performs a thresholding operation on the variables that yield the latent \mathbf{z} and output \mathbf{y} vectors that are learned through observations drawn from the training data-set. This in turn makes the models highly non-linear [36]. An algebraic expression of the ReLU function that is related to the concept of thresholding of negative values is presented in [37]. In [37][Sec. 3, Eq. (3)], a single application of the ReLU function for a given input vector $\tilde{\mathbf{x}}$ can be expressed as a *binary diagonal* matrix, that sets to 0 any negative value of the encoded vector and we denote that matrix as \mathbf{G} . Consequently, to obtain the couplings matrix of the DAE, MSS-DAE, and SF models it is necessary to compute as many matrices \mathbf{G} as the number of application of the ReLU function in the DAE, MSS-DAE, and SF models:

$$\mathbf{C}^o = \mathbf{G}_{\text{dec}} \mathbf{W}_{\text{dec}} \dots \mathbf{G}_{\text{enc}} \mathbf{W}_{\text{enc}}. \quad (14)$$

Furthermore, to compute each matrix \mathbf{G}_* in Eq. (14), it is necessary to learn the model specific dependencies that are captured by the DAE, MSS-DAE, and SF models during the supervised training [36, 37]. The data dependencies

expressed by each \mathbf{G}_* refer to the algebraic operations between the mixture $\tilde{\mathbf{x}}$ or the corresponding latent vectors \mathbf{z} , i.e., the encoding or decoding matrices \mathbf{W}_* , and the corresponding bias terms \mathbf{b}_* as in Eqs. (4)–(10). The asterisk “*” is used for brevity, and replaces the subscripts and/or superscripts of the layer identifiers initially used in Eqs. (4)–(9).

A straightforward way to learn the data dependencies can be derived from the knowledge distillation concept presented in [29]. In knowledge distillation, a neural network, i.e., the *student*, is optimized to predict the output of a more complicated model (e.g. the non-linear DAE, MSS-DAE and SF). Subject to the goal of this work, we restrict the student network to be a linear, affine transformation from $\tilde{\mathbf{x}}$ to \mathbf{y} . That transformation is based on the product of the mixture spectra $\tilde{\mathbf{x}}$ and the couplings matrix \mathbf{C} . For computing the couplings matrix \mathbf{C} we propose to solve the following optimization problem:

$$\mathbf{C}^o = \underset{\mathbf{C}}{\operatorname{argmin}} \|\mathbf{y} - \mathbf{C}\tilde{\mathbf{x}}\|, \text{ where} \quad (15)$$

$\|\cdot\|$ is the ℓ_1 norm and $\tilde{\mathbf{x}}$ is sampled from the testing data-set. The output vector \mathbf{y} is computed by using $\tilde{\mathbf{x}}$ as an input to the corresponding model. The ℓ_1 norm is used due to the sparse nature of magnitude spectral data. Given that Eq. (15) is inspired by the student network of the knowledge distillation concept [29], we will denote this strategy as the *student*.

To compute \mathbf{C}^o , the student strategy employs the following partial derivatives, with E denoting the error of the ℓ_1 norm contained in Eq.(15):

$$\Delta := \frac{\partial E}{\partial \mathbf{C}} = \frac{\partial E}{\partial \mathbf{C}\tilde{\mathbf{x}}} \frac{\partial \mathbf{C}\tilde{\mathbf{x}}}{\partial \mathbf{C}} \quad (16)$$

From Eq. (16), it follows that the gradient signal Δ that is used to update \mathbf{C} in an iterative manner is given by $\Delta = \operatorname{sgn}(\mathbf{C}\tilde{\mathbf{x}} - \mathbf{y})\tilde{\mathbf{x}}^T$, where sgn is the signum element-wise function and \cdot^T is the vector/matrix transposition. The gradient signal Δ suggests that the optimal \mathbf{C}^o lies over the least affinity between the mixture magnitude spectra $\tilde{\mathbf{x}}$ and $\mathbf{C}\tilde{\mathbf{x}} - \mathbf{y}$. This means that the updates of \mathbf{C} only favor the minimization of the above mentioned reconstruction error term. Although this strategy could yield simplified and robust surrogates of possibly deep and complex models for source separation (in terms of reconstruction errors) [29], it neglects the learned data dependencies contained in the encoding and decoding matrices of Eq. (14). Given that our goal is to include the knowledge captured by the encoding/decoding matrices \mathbf{W}_* and bias terms \mathbf{b}_* , we propose an alternative strategy that we denote as *compositional*. The proposed strategy composes the couplings matrix \mathbf{C} similar to the composition expressed in Eq. (14). It also uses \mathbf{G}_* for extracting the above mentioned data dependencies contained in each \mathbf{W}_* . More specifically, we exploit the fact that the ReLU function behaves linearly in the non-negative range where the mixture $\tilde{\mathbf{x}}$, the output \mathbf{y} , and the latent \mathbf{z} vectors reside in. Therefore, and according to Eqs. (4)–(9), the relevant components that affect which elements are thresholded by the ReLU function for computing the latent \mathbf{z} and output \mathbf{y} vectors, are the row-vectors contained in each \mathbf{W}_* and the corresponding bias term(s) \mathbf{b}_* .

Inspired by [37], that models the ReLU function as a diagonal matrix \mathbf{G}_* that scales the row-vectors of \mathbf{W}_* in Eq. (14), we build the couplings matrix for the compositional strategy as follows:

$$\mathbf{C} = (\mathbf{G}_{\text{dec}} \odot \mathbf{W}_{\text{dec}}) \dots (\mathbf{G}_{\text{enc}} \odot \mathbf{W}_{\text{enc}}). \quad (17)$$

The Hadamard product in Eq. (17) accounts for each individual element of the row vectors contained in the corresponding \mathbf{W}_* , rather than having a single scalar value per row-vector as in the case of the diagonal matrix. The reason is that the sign and the magnitude of the elements in each \mathbf{W}_* carry essential information in the model-dependent processing of non-negative vectors. For considering the influence of the sign of the elements in each \mathbf{W}_* , we restrict each matrix \mathbf{G}_* to be non-negative, i.e., $\mathbf{G}_* \in \mathbb{R}_{\geq 0}^{N \times N}$.

To do so, and to account for the influence of the bias terms we compute each \mathbf{G}_* using:

$$\mathbf{G}_* = g(\hat{\mathbf{G}}_*) \quad (18)$$

$$\hat{\mathbf{G}}_* = \mathbf{P}_*(\mathbf{W}_* + \mathbf{b}_*)^T. \quad (19)$$

The elements in \mathbf{W}_* are either preserved and scaled or nullified by \mathbf{G}_* . This depends on their relevance for mapping the mixture magnitude spectra under linear constraints. This is done by using matrix \mathbf{C} to the optimization problem defined in Eq. (15). The unknowns in the compositional strategy are the matrices \mathbf{P}_* , that are jointly optimized using the back-propagation method.

To further analyze how the previously stated data dependencies are learned using the compositional strategy, let us consider the case in which a single encoding and decoding matrix is used, as in the DAE and SF models. In that case, for the compositional strategy it is required to compute two matrices \mathbf{P}_{enc} and \mathbf{P}_{dec} . The corresponding partial derivatives are defined as $\frac{\partial E}{\partial \mathbf{P}_{\text{dec}}} = \frac{\partial E}{\partial \mathbf{C}} \frac{\partial \mathbf{C}}{\partial \mathbf{G}_{\text{dec}}} \frac{\partial \mathbf{G}_{\text{dec}}}{\partial \mathbf{P}_{\text{dec}}}$, and $\frac{\partial E}{\partial \mathbf{P}_{\text{enc}}} = \frac{\partial E}{\partial \mathbf{C}} \frac{\partial \mathbf{C}}{\partial \mathbf{G}_{\text{enc}}} \frac{\partial \mathbf{G}_{\text{enc}}}{\partial \mathbf{P}_{\text{enc}}}$, respectively. Using Eq.(16) the aforementioned

Algorithm 1 The Neural Couplings Algorithm

Require: Mixture spectra $\tilde{\mathbf{x}}$, model $\mathcal{M}(\cdot)$, model's parameters $\mathbf{W}_*, \mathbf{b}_*$, $N \times N$ identity matrix \mathbf{I}_N , total number of layers in model L' , number of iterations N_{it} , strategy $S \in \{\text{student, compositional}\}$, random generator function rnd , optimizer/solver $\mathcal{A}(\cdot)$

- 1: $\mathbf{y} \leftarrow \mathcal{M}(\tilde{\mathbf{x}})$
- 2: **if** S is *student* **then**
- 3: $\mathbf{C} \leftarrow rnd$
- 4: **else**
- 5: $\mathbf{C} \leftarrow \mathbf{I}_N$
- 6: **for** $l' := 1$ **to** L' **do**
- 7: $\mathbf{P}_{l'} \leftarrow rnd$
- 8: $\mathbf{G}_{l'} \leftarrow g(\mathbf{P}_{l'}(\mathbf{W}_{l'} + \mathbf{b}_{l'})^T)$
- 9: $\mathbf{C} \leftarrow (\mathbf{W}_{l'} \odot \mathbf{G}_{l'})\mathbf{C}$
- 10: **end for**
- 11: **end if**
- 12: **for** $i := 1$ **to** N_{it} **do**
- 13: $E \leftarrow \|\mathbf{y} - \mathbf{C}\tilde{\mathbf{x}}\|$
- 14: **if** S is *student* **then**
- 15: $\mathbf{C} \leftarrow \mathbf{C} - \mathcal{A}(\frac{\partial E}{\partial \mathbf{C}})$
- 16: **else**
- 17: $\mathbf{C} \leftarrow \mathbf{I}_N$
- 18: **for** $l' := 1$ **to** L' **do**
- 19: $\mathbf{P}_{l'} \leftarrow \mathbf{P}_{l'} - \mathcal{A}(\frac{\partial E}{\partial \mathbf{P}_{l'}})$
- 20: $\mathbf{G}_{l'} \leftarrow g(\mathbf{P}_{l'}(\mathbf{W}_{l'} + \mathbf{b}_{l'})^T)$
- 21: $\mathbf{C} \leftarrow (\mathbf{W}_{l'} \odot \mathbf{G}_{l'})\mathbf{C}$
- 22: **end for**
- 23: **end if**
- 24: $\mathbf{C}^o \leftarrow \mathbf{C}$
- 25: **end for**
- 26: **return** \mathbf{C}^o

partial derivatives are as follows:

$$\frac{\partial E}{\partial \mathbf{P}_{\text{dec}}} = (\Delta(\mathbf{W}_{\text{enc}} \odot \mathbf{G}_{\text{enc}}) \odot \mathbf{W}_{\text{dec}} \odot g'(\hat{\mathbf{G}}_{\text{dec}}))(\mathbf{W}_{\text{dec}} + \mathbf{b}_{\text{dec}}) \quad (20)$$

$$\frac{\partial E}{\partial \mathbf{P}_{\text{enc}}} = ((\mathbf{W}_{\text{dec}} \odot \mathbf{G}_{\text{dec}})^T \Delta \odot \mathbf{W}_{\text{enc}} \odot g'(\hat{\mathbf{G}}_{\text{enc}}))(\mathbf{W}_{\text{enc}} + \mathbf{b}_{\text{enc}}), \quad (21)$$

where $g'(x)$ is the first derivative of the ReLU element-wise function, that is approximated by a function that is equal to 1 for positive inputs and 0 otherwise.

\mathbf{G}_{dec} and \mathbf{G}_{enc} are computed using Eq.(19). In Eqs. (20) and (21) instead of taking into account only the gradient for minimizing the reconstruction error, i.e., Δ , the models' optimized parameters \mathbf{W}_* and \mathbf{b}_* are considered by using the dot products between the two groups of parentheses that surround the encoding and decoding matrices, similar to the linear composition of Eqs. (11)–(13). The Hadamard products including the $g'(x)$ inside the first parentheses of Eqs. (20) and (21) can be understood as the search of elements contained in the decoder and encoder matrices, that are contributing to the mapping of the mixture to the corresponding output. From the above, it can be said that the compositional strategy applies a layer-wise restriction, compared to the student strategy that does not take into account the information in each \mathbf{W}_* and \mathbf{b}_* . The restriction forces the couplings matrix to be computed using the parameters of each model, similar to the linear composition that algebraically corresponds to the mapping function. It should be mentioned that regardless the strategy (i.e., student and compositional), the computed matrices \mathbf{C}_* are allowed to retain negative values. That is because the destructive property of the negatives values during the computation of the vector-matrix products are helpful in estimating the target source's magnitude information. The pseudo-algorithm of the NCA for both strategies is given in Algorithm 1.

4 Experimental Procedure

4.1 Training & Assessing the Source Separation Models

For optimizing the parameters contained in Eqs. (5)–(9), we use the 100 two-channel multi-tracks available in the MUSDB18 data-set [38] that have been used in the SiSEC 2018 campaign [3]. The multi-track recordings are sampled at 44100 Hz. For each multi-track, we use the mixture and singing voice signals in the data-set, and average the two available channels, i.e., monaural mixing. To construct the data-set \mathcal{D} , the STFT analysis is performed for each mixture and corresponding source signal, using the hamming windowing 46 ms long, a factor of 2 for zero-padding, a hop-size of 8.7 ms, and a frequency analysis of $N' = 4096$ from which only the first $N = 2049$ frequency sub-bands are retained (due to the redundancies of the discrete Fourier decomposition). After computing the magnitude of the complex representation each frequency sub-band is normalized to have a unit variance with respect to the time-frames.

We use a single encoding and decoding layer for all models in all approaches. The number of hidden layers for MSS-DAE is set to $L = 2$ (MSS-DAE has $L' = 4$ layers in total). The dimensionality through the layers is preserved the same in order to avoid any implicit model regularization [5, 4, 23]. The number of layers for MSS-DAE model was chosen experimentally according to the saturation in minimizing Eq. (3) during the training process, with respect to the number of hidden layers. All the weight matrices are initialized with samples drawn from a normal distribution and scaled by $\sqrt{\frac{1}{N}}$ as proposed in [39]. The bias terms are initialized to zero. The data-set \mathcal{D} is randomly shuffled, and the training is performed using batches of 128 time-frames. For gradient based optimization, the Adam algorithm [40] is used with the initial learning rate set to $1e - 3$, and decreased by half if no improvement to the loss was observed for two consecutive iterations over all available training data. The exponential decay rates for the first and second-order moments of the Adam algorithm are set to 0.9 and 0.999, respectively. The training is terminated after no improvement is observed over four consecutive iterations throughout the training data. We iterate through the whole model training procedure 50 times using different random initialization states. All our experiments are carried out using NVIDIA's GeForce GTX Titan X and the PyTorch framework².

To assess the source separation models, we focus on evaluating the ability of each model to exploit the structure in music spectral representations. To do so, we use the couplings matrix computed with the NCA, which acts as a data and model-specific filtering operator. According to [34], there are two broad classes of filtering operators. The first class is the *vector* filtering operator, where the matrix responsible for filtering, i.e., the couplings matrix, contains high values of magnitude on off-diagonal elements. The main benefit of off-diagonal elements is that they allow the exploitation of inter-frequency relationships of the spectral data. In contrast, the second class of filtering operators is denoted as *scalar* filters. Scalar filters are characterized by magnitude only on the main diagonal of the couplings matrix. Each element on the main diagonal scales individually the corresponding frequency sub-band. The latter operation is equivalent to the application of a masking strategy [25]. In practice, source separation models are optimized using substantially many training examples. Consequently, learning a mapping function with activity on the main diagonal could imply a limited performance in estimating the singing voice spectra.

Based on the previous argument, we define an objective measure that denoted the *trace-to-off-diagonal-ratio* (TOD-R). The TOD-R is computed as follows:

$$\text{TOD-R}(\mathbf{C}_*) = \sqrt{N} \frac{\text{tr}(|\mathbf{C}_*|)}{\|\mathbf{C}_* \odot (\mathbf{J}_N - \mathbf{I}_N)\|}, \quad (22)$$

where $\text{tr}(\cdot)$ is the trace function that adds up all the elements on the main diagonal of the matrix, \mathbf{I}_N is the $N \times N$ identity matrix, and \mathbf{J}_N is the $N \times N$ with all elements equal to one. The scaling by \sqrt{N} is performed in order to compensate for the initialization scaling described before, and due to the expected high values of the denominator in Eq. (22) (since the norm is taken using far more matrix elements than the trace in the numerator). The element-wise absolute $|\cdot|$ is computed prior to the computation of the trace, to avoid biasing the ratio due to the norm (sum of absolute values) in the denominator of Eq. (22). Small values of TOD-R indicate that the off-diagonal elements of the couplings matrix retain higher magnitude values than the elements on the main diagonal and vice versa. High off-diagonal activity suggests that the mapping function of the model exploits more inter-frequency relationships rather than estimating values that scale the mixture spectra as in scalar-based filtering and frequency masking [34].

4.2 Computing & Assessing the Neural Couplings

For computing the neural couplings, i.e., solving the optimization problem in Eq.(15), we use the test subset from the MUSDB18 data-set [38]. The test subset comprises 50 additional two-channel, multi-tracks sampled at 44100

²<https://pytorch.org/>

Hz. For computing the STFT we employed the same parameters as during the construction of the training data-set \mathcal{D} reported in Sec.4.1. As it is more informative to compute mapping functions that process multiple time-frame vectors rather than a single instance, we use a batch of adjacent magnitude vectors drawn from the test subset. The batch size is set to $T = 350$ (~ 3.1 seconds long), and the hyper-parameter T is experimentally chosen based on the trade-off between the number of vectors and computational resources. With this, we can simply reformulate the NCA using matrix notation instead of vector notation, i.e., $\tilde{\mathbf{X}} \in \mathbb{R}_{\geq 0}^{N \times T}$ instead of $\tilde{\mathbf{x}} \in \mathbb{R}_{\geq 0}^N$ and $\mathbf{Y} \in \mathbb{R}_{\geq 0}^{N \times T}$ instead of $\mathbf{y} \in \mathbb{R}_{\geq 0}^N$. For the solver denoted as $\mathcal{A}(\cdot)$ in Algorithm 1, we use the Adam algorithm with a fixed learning rate equal to $4e^{-4}$ and the same exponential decay rates as in 4.1. The total number of iterations is set to 600, and the random function (rnd in Algorithm 1) refers to drawing samples from a normal distribution scaled by $\sqrt{\frac{1}{N}}$ as proposed in [39].

In our initial experiments it was observed that many silent segments in the multi-tracks of our test-set led to sparse and randomly structured \mathbf{C}^o matrices for the three models. This sparse and random structure significantly biases the TOD-R measure in an unpredictable manner. Therefore, from each multi-track we select the 30 seconds that all music sources available in the data-set are active. The selection of the active waveform regions, is based on the generator³ used in the music source separation evaluation campaign [3]. The pre-trained parameters of each one of the three models are randomly drawn from one of the 50 training instances.

As we have not provided any theoretical guarantees regarding the convergence of the NCA to an optimal solution, we further assess the NCA for each strategy, model, and segmented multi-track. This is done by computing a divergence metric between the singing voice spectra estimated by the NCA, and the singing voice spectra estimated by the corresponding model. The divergence metric is the logarithmic, generalized Kullback-Leibler divergence (log-KL), previously proposed for assessing the performance of music spectrogram in-painting methods [41], and is computed for evaluating the strategies using:

$$\mathcal{L}_{\log\text{-KL}}(\mathbf{X}, \hat{\mathbf{X}}) = \log(\|\mathbf{X} \odot \log(\frac{\mathbf{X}}{\hat{\mathbf{X}}}) - \mathbf{X} + \hat{\mathbf{X}}\|), \quad (23)$$

where \log is the element-wise logarithmic function. By minimizing Eq. (23) the estimates $\hat{\mathbf{X}}$ become closer to the target spectra \mathbf{X} .

5 Results & Discussion

To address our research question “**RQ2: Do DAEs that are commonly employed in music source separation learn trivial solutions for the given problem?**”, we compute the linear composition functions for the three models (DAE, MSS-DAE, and SF) using Eqs. (11)–(13). The computation of the linear compositions follows the research findings presented in [23] that underlines the tendency of encoding and decoding functions to become symmetric, that practically leads to learning scalar filtering operators. The average result, across the 50 experimental iterations, from the composition functions is illustrated in Fig.2. By observing Fig.2 it is evident that the two models that map directly the mixture magnitude spectra to the singing voice spectra (DAE and MSS-DAE) have a prominent main diagonal structure. This means that through training, the corresponding encoding and decoding functions tend to become symmetric in order to provide a solution in the MSE sense. Therefore, it is plausible that the DAE and MSS-DAE models learned trivial solutions to the problem of singing voice separation, restricting the overall performance of separation. On the other hand, employing the skip-connections as performed for the SF model, it can be observed from the right column of Fig.2 that the activity has been repelled from the main diagonal. This can be explained by recalling that a solution for estimating the singing voice spectra is the scaling the individual frequency sub-bands of the mixture, which in turn is expressed by a diagonal matrix. That statement provides a simple explanation on why skip-connections [42] and end-to-end learning [43], where the time-domain signals are used instead of spectrograms, are emerging directions in music source separation.

Aiming to address the other research question “**RQ1: Why is masking important in approaches based on the DAE model?**”, we turn our focus to the computed mapping functions using the NCA, and the model assessment via the TOD-R metric. Table 1 summarizes the TOD-R results for each model, both for the student and the compositional strategies. The average TOD-R across all the segments of the test-subset is reported, and in the parentheses the standard deviation of the corresponding measurements is provided. Bold faced numbers, indicate the smallest obtained value for the TOD-R implying that the model has exploited a richer inter-frequency structure.

The results of Table 1 show that the SF model, for both strategies, provides the smallest TOD-R value. More specifically, the TOD-R for the compositional strategy and the SF model is 12 times smaller than the DAE model, which has

³Available at: <https://github.com/sigsep/sigsep-mus-cutlist-generator>

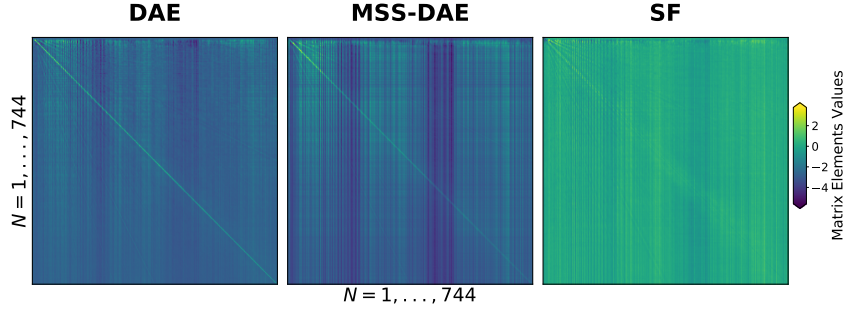


Figure 2: The linear composition of the models’ encoding and decoding functions. The compositions are computed using the Eqs. (11)–(13), and averaged across the 50 experimental iterations. The first 744 frequency sub-bands ($\sim 8\text{kHz}$) are displayed for clarity. *Left Column*: Composition for the denoising auto-encoder model [4] (DAE). *Middle Column*: Composition for the four layer extension of the DAE model, adapted to music source separation (MSS-DAE) [19, 22]. *Right Column*: Composition for the skip connections for filtering the input mixture (SF) [14, 12, 15].

Table 1: Assessing the mapping functions. The TOD-R metric (Eq. (22)) for each strategy and model.

Strategy	Model		
	DAE	MSS-DAE	SF
Student	0.03 (± 0.00)	0.03 (± 0.00)	0.02 (± 0.00)
Compositional	0.36 (± 0.13)	0.14 (± 0.04)	0.03 (± 0.01)

equal number of encoding and decoding layers. In comparison to the MSS-DAE model that comprises 2 additional hidden layers, the TOD-R value of the SF model is decreased by approximately 4.6 times. We could conclude that skip connections can be seen as a simple method to repel source separation approaches from learning solutions that concentrate most of the activity on the main diagonal of their corresponding mapping function(s).

Additionally, Table 2 presents the results of the reconstruction performance evaluation of the NCA strategies according to the divergence metric in Eq. (23). For comparison, we report the reconstruction performance of the linear composition and the identity function as baseline estimates of each model’s mapping function. The overall reconstruction performance of the NCA outperforms the linear composition by ~ 5 times and the identity function by ~ 1.9 times in terms of the $\mathcal{L}_{\log\text{-KL}}$. This indicates that the NCA provides accurate approximations of the source separation models magnitude spectral information. The student strategy marginally outperforms the compositional strategy by an average factor of 0.1. This is due to the fact that the student strategy employs gradient updates that are related only to the reconstruction error minimization.

Focusing on the structure of the mapping functions that are computed using the NCA via the student strategy, illustrated in the first row of Fig.3, it can be seen that the couplings matrices, serving as the corresponding mapping functions, are nearly identical between the DAE and MSS-DAE models, and marginally different from the SF model. The marginal differences can be explained by the fact that the couplings matrix for the SF model was optimized, according to Eq.(15) using the output masks of the SF model as target function(s) \mathbf{Y} , as opposed to the DAE and MSS-DAE models that use the corresponding singing voice spectral estimates as target function(s).

The above tendency is also demonstrated in Table 1, where the statistics of the TOD-R metric for the student strategy are exactly the same for the DAE and the MSS-DAE models. This shows that the mappings are nearly identical between the models. An explanation to that is by recalling the Eqs. (15)–(16) that depict the approximation of the mapping functions being performed by observing only input-output and model-dependent relationships of spectral representations, neglecting the parameters of the model. Recalling that each model is initially optimized to estimate the singing voice spectra using Eq. (3) and the same training data as the rest of the models, only spectral-dependent computations (i.e., neglecting Eq. (14)) of the mapping function(s) introduce ambiguities with respect to the examination of what each source separation model has learned. Consequently, we turn our focus on the compositional strategy, that includes the knowledge of the parameters of each model. In the second row of Table 1 and Figs. 3.d–3.e, a pattern that is evident among the mapping functions of the DAE and MSS-DAE models, is the high diagonal activity when compared to the SF model that employs the skip connections. Specifically, the mapping function of the SF model has pushed most of its activity away from the main diagonal. For small N , i.e., in the first matrix rows of the zoomed mapping function of Fig.3.f, it can be seen that elementary spectral structures are formed. Those spectral structures are related to the

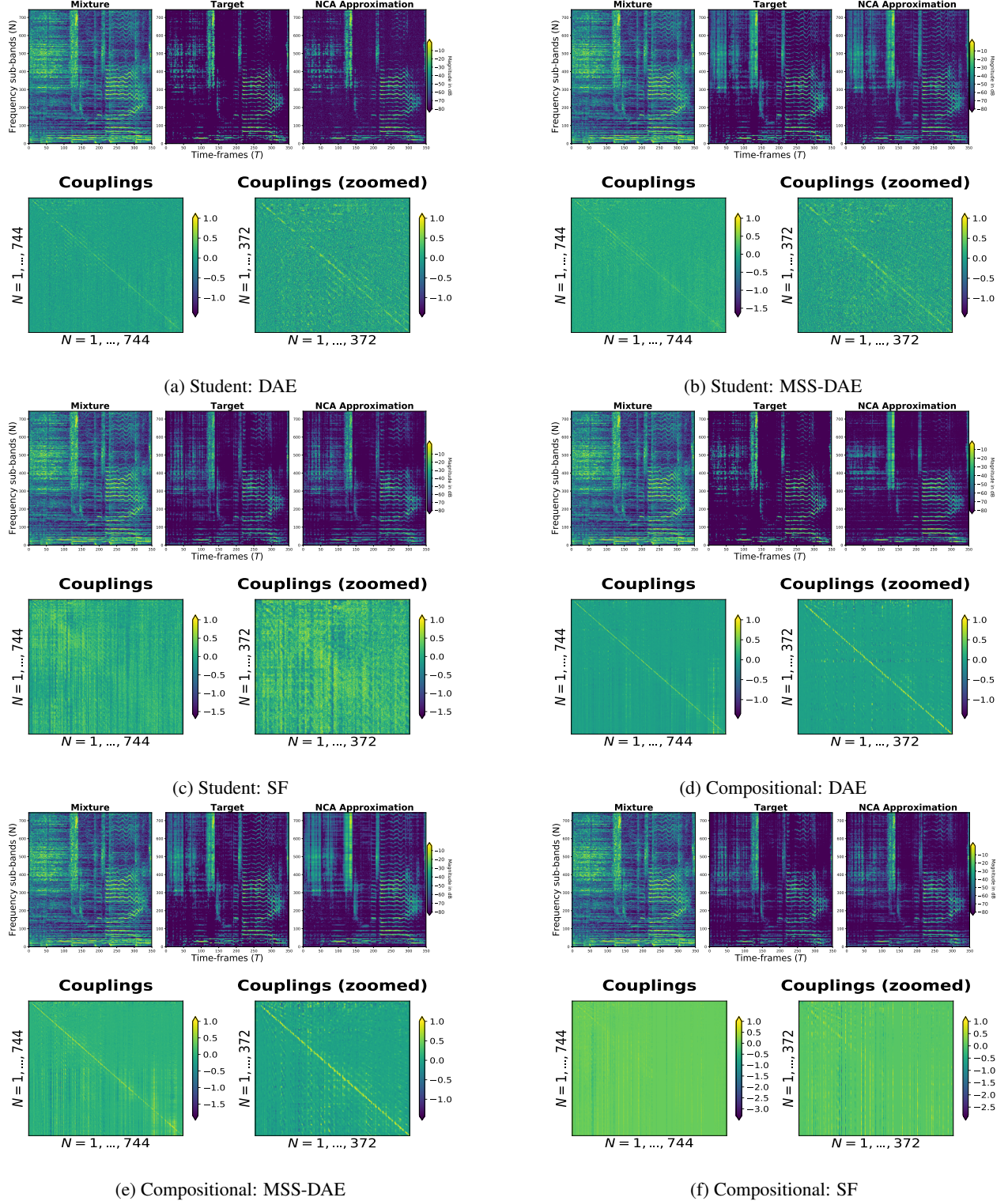


Figure 3: The outcome of the NCA for the DAE, MSS-DAE, and SF models using a ~ 3 seconds excerpt from the file *Al James - Schoolboy Fascination* contained in the test sub-set of MUSDB18. *First Row (a)–(c)*: The couplings matrices approximating the mapping functions and the corresponding spectral estimates using the *student* strategy. *Second Row (d)–(f)*: The couplings matrices approximating the mapping functions and the corresponding spectral estimates using the *compositional* strategy. A row-wise maximum value normalization, and zooming of the couplings matrices is illustrated for clarity.

Table 2: Assessing the reconstruction performance using the logarithmic, generalized Kullback-Leibler divergence (Eq. 23) of the mappings computed by NCA against the identity and the linear composition functions. The average values and standard deviations are reported across the test set.

Strategy	Model		
	DAE	MSS-DAE	SF
Student	2.77(±0.25)	2.32(±0.22)	2.57(±0.29)
Compositional	2.81(±0.28)	2.15(±0.24)	2.73(±0.31)
Baseline	DAE	MSS-DAE	SF
Linear Comp.	11.32(±0.22)	7.00(±0.56)	21.15(±0.67)
Identity Funct.	4.92(±0.34)	4.92(±0.34)	4.92(±0.34)

target spectra of Fig.3.f as both the spectral and the mapping function illustrations concentrate magnitude information in same frequency sub-band regions. According to the graphical model and its expected conditional, i.e., Fig.1.c and $q(x|\tilde{x})q(\tilde{x})$, we can underline that the mapping function of the SF model captures the relevant structure of the target source that has been observed in the mixture such that a time-frequency mask can be applied to suppress the interfering sources. What is not evident in our results, is the SF model’s capacity in learning spectral structures from the training data.

To this end, Fig. 3 also shows that the additional layers that the MSS-DAE model employs are essentially used to model additional inter-frequency relationships, compared to the DAE model that comprises only two layers and concentrates most of its activity on the main diagonal. However, the MSS-DAE model not only pushes its activity to off-diagonal elements but also forms a structured matrix, mostly seen in the zoomed couplings matrix of Fig.3.e, that is *roughly* similar to a circulant matrix with sparse entries. Those types of matrices are commonly used in digital signal processing for convolutional operators. That observation somewhat justifies the advantage of incorporating additional computational layers into a source separation model as proposed in [22, 19] and serves as an explanation on why convolutional layers are attractive choices in source separation models [21].

6 Conclusions & Future Research

In this study we formalized two research questions regarding the most commonly used neural network model in music source separation, i.e., the denoising autoencoder presented in [4]. Our two research questions were: *RQ1* “*Why is masking important in approaches based on the DAE model?*”, and *RQ2* “*Do DAEs that are commonly employed in music source separation learn trivial solutions for the given problem?*”. To answer those questions we focused on the examination of the mapping functions of the corresponding model. For computing the mapping functions, we proposed an experimentally derived algorithm and investigated two strategies to that aim. The first one, denoted as the *student strategy*, is based on the neural network distillation concept presented in [29]. It was observed that the student strategy leads to ambiguous results regarding the approximation of the mapping functions as it does not account for the model’s parameters. As an alternative, the *compositional strategy* was proposed for taking into account the model’s already optimized parameters for the problem of singing voice separation, similarly to the algebraic derivation of the mapping function.

Using the compositional strategy and the computed mapping functions we investigated the denoising autoencoder (DAE) model, its multi-layered extension employed in relevant tasks [22, 19, 20] (MSS-DAE), and the denoising autoencoder with skip-connections (SF) that are used to mask the mixture spectra similarly to a time-frequency filtering operation [14, 12, 15]. By examining the overall structure of the mapping functions, we conclude that the source separation models learn data-driven filtering functions. The DAE model learns trivial solutions because the corresponding encoding and decoding functions become symmetric during the training procedure. Consequently, the learned, by the DAE, filtering functions act as scalar filters in the frequency domain potentially limiting the overall source estimation performance. Furthermore, employing skip-connections as in the SF model, it can be seen as a simple method to enforce DAEs to learn richer inter-frequency dependencies as opposed to the DAE. That can justify the empirically observed performance boost over DAEs in previous works like [12, 17, 15, 18]. Finally, the additional computational layers employed in the MSS-DAE model, seem to promote the learning of filter kernels with a sparse and circulant structure roughly similar to convolutional operations. However, those kernels share also similarities with scalar filters, as in the case of the DAE, that reduce the overall filtering performance and supporting the experimental results in [19] that promote the usage of masking as a post-processing step for estimating the target source(s).

Directions for future research include the linking between the demonstrated mapping functions and the spectral transportation matrices [28]. That could assist in a geometrical understanding of denoising functions in deep learning based signal separation. Furthermore, examining another important type of skip connections that are commonly referred to as residual connections is of high importance, as residual connections play an important role in signal enhancement and denoising [21, 42]. Finally, expanding the proposed study to more advanced architectures, is also emerging. It should be stated though, that the mappings for recurrent and convolutional neural networks are not expected to deviate significantly from the mappings presented in this work, since the signal estimation is based on vector and matrix products as the models examined in this work. The code for reproducing the above results and computing the gradients can be found under: <https://zenodo.org/record/2629650>.

Acknowledgments

The research leading to these results has received funding from the European Union’s H2020 Framework Programme (H2020-MSCA-ITN-2014) under grant agreement no 642685 MacSeNet. Stylianos Ioannis Mimilakis is supported by the by the German Research Foundation (AB 675/2-1, MU 2686/11-1). The authors would like to thank Rodrigo Pena (EPFL), Derry Fitzgerald (AudioSourceRE), Paul Magron (Tampere University), and Luca Cuccovillo (Fraunhofer-IDMT) for the fruitful discussions.

References

- [1] D. Wang and J. Chen, “Supervised speech separation based on deep learning: An overview,” *IEEE/ACM Transactions on Audio, Speech, and Language Processing*, vol. 26, no. 10, pp. 1702–1726, Oct 2018.
- [2] Z. Rafii, A. Liutkus, F. R. Stöter, S. I. Mimilakis, D. FitzGerald, and B. Pardo, “An overview of lead and accompaniment separation in music,” *IEEE/ACM Transactions on Audio, Speech, and Language Processing*, vol. 26, no. 8, pp. 1307–1335, Aug 2018.
- [3] F.-R. Stöter, A. Liutkus, and N. Ito, “The 2018 Signal Separation Evaluation Campaign,” in *Proceedings of the Latent Variable Analysis and Signal Separation: 14th International Conference on Latent Variable Analysis and Signal Separation*, Surrey, United Kingdom, Jul. 2018.
- [4] P. V. H. Larochelle and P.-A. M. Y. Bengio, “Extracting and composing robust features with denoising autoencoders,” in *Proceedings of the 25th International Conference on Machine Learning (ICML)*. New York, NY, USA: ACM, 2008, pp. 1096–1103.
- [5] P. Vincent, H. Larochelle, I. Lajoie, Y. Bengio, and P.-A. Manzagol, “Stacked denoising autoencoders: Learning useful representations in a deep network with a local denoising criterion,” *Journal of Machine Learning Research*, vol. 11, pp. 3371–3408, 2010.
- [6] E. M. Grais, G. Roma, A. J. R. Simpson, and M. D. Plumbley, “Two-stage single-channel audio source separation using deep neural networks,” *IEEE/ACM Transactions on Audio, Speech, and Language Processing*, vol. 25, no. 9, pp. 1773–1783, Sept 2017.
- [7] D.-S. Williamson, Y. Wang, and D. Wang, “Complex ratio masking for monaural speech separation,” *IEEE/ACM Transactions on Audio, Speech, and Language Processing*, vol. 24, no. 3, pp. 483–492, March 2016.
- [8] Y. Wang, A. Narayanan, and D. Wang, “On training targets for supervised speech separation,” *IEEE/ACM Transactions on Audio, Speech, and Language Processing*, vol. 22, no. 12, pp. 1849–1858, Dec 2014.
- [9] A. Liutkus and R. Badeau, “Generalized Wiener filtering with fractional power spectrograms,” in *Proceedings of the 40th International Conference on Acoustics, Speech and Signal Processing (ICASSP 2015)*, Apr. 2015, pp. 266–270.
- [10] S. Voran, “The selection of spectral magnitude exponents for separating two sources is dominated by phase distribution not magnitude distribution,” in *Proceedings of the 2017 IEEE Workshop on Applications of Signal Processing to Audio and Acoustics (WASPAA 2017)*, Oct. 2017.
- [11] D. FitzGerald and R. Jaiswal, “On the use of masking filters in sound source separation,” in *Proceedings of the 15th International Conference on Digital Audio Effects (DAFx-12)*, Sep. 2012.
- [12] F. Weninger, J. R. Hershey, J. L. Roux, and B. Schuller, “Discriminatively trained recurrent neural networks for single-channel speech separation,” in *Proceedings of the 2014 IEEE Global Conference on Signal and Information Processing (GlobalSIP)*, Dec 2014, pp. 577–581.

- [13] P.-S. Huang, M. Kim, M. Hasegawa-Johnson, and P. Smaragdis, “Joint optimization of masks and deep recurrent neural networks for monaural source separation,” *IEEE/ACM Transactions on Audio, Speech, and Language Processing*, vol. 23, no. 12, pp. 2136–2147, Dec. 2015.
- [14] S.-I. Mimilakis, K. Drossos, G. Schuller, and T. Virtanen, “A recurrent encoder-decoder approach with skip-filtering connections for monaural singing voice separation,” in *Proceedings of the 27th IEEE International Workshop on Machine Learning for Signal Processing (MLSP)*, 2017.
- [15] A. Jansson, E. Humphrey, N. Montecchio, R. Bittner, A. Kumar, and T. Weyde, “Singing voice separation with deep U-Net convolutional networks,” in *Proceedings of the 18th International Society for Music Information Retrieval Conference*, Suzhou, China, Oct. 2017.
- [16] J. Lee, J. Skoglund, T. Shabestary, and H. Kang, “Phase-sensitive joint learning algorithms for deep learning-based speech enhancement,” *IEEE Signal Processing Letters*, vol. 25, no. 8, pp. 1276–1280, Aug 2018.
- [17] S. I. Mimilakis, K. Drossos, J. F. Santos, G. Schuller, T. Virtanen, and Y. Bengio, “Monaural singing voice separation with skip-filtering connections and recurrent inference of time-frequency mask,” in *Proceedings of the 43rd International Conference on Acoustics, Speech and Signal Processing (ICASSP 2018)*, 2018.
- [18] K. Drossos, S. I. Mimilakis, D. Serdyuk, G. Schuller, T. Virtanen, and Y. Bengio, “MaD TwinNet: Masker-denoiser architecture with twin networks for monaural sound source separation,” in *Proceedings of the 2018 IEEE International Joint Conference on Neural Networks (IJCNN)*, July 2018.
- [19] S. Uhlich, F. Giron, and Y. Mitsufuji, “Deep neural network based instrument extraction from music,” in *Proceedings of the 40th International Conference on Acoustics, Speech and Signal Processing (ICASSP 2015)*, 2015, pp. 2135–2139.
- [20] S. Uhlich, M. Porcu, F. Giron, M. Enenkl, T. Kemp, N. Takahashi, and Y. Mitsufuji, “Improving music source separation based on deep neural networks through data augmentation and network blending,” in *Proceedings of the 42nd International Conference on Acoustics, Speech and Signal Processing (ICASSP 2017)*, 2017, pp. 261–265.
- [21] N. Takahashi and Y. Mitsufuji, “Multi-scale multi-band densenets for audio source separation,” in *Proceedings of the 2017 IEEE Workshop on Applications of Signal Processing to Audio and Acoustics (WASPAA 2017)*, Oct. 2017.
- [22] A. A. Nugraha, A. Liutkus, and E. Vincent, “Multichannel music separation with deep neural networks,” in *Proceedings of the 24th European Signal Processing Conference (EUSIPCO)*, Aug 2016, pp. 1748–1752.
- [23] D. J. Im, M. I. Belghazi, and R. Memisevic, “Conservativeness of untied auto-encoders,” in *Proceedings of the 30th AAAI Conference on Artificial Intelligence*, 2016.
- [24] J. Särälä and H. Valpola, “Denoising source separation,” *J. Mach. Learn. Res.*, vol. 6, pp. 233–272, Dec. 2005.
- [25] H. Erdogan, J. R. Hershey, S. Watanabe, and J. L. Roux, “Phase-sensitive and recognition-boosted speech separation using deep recurrent neural networks,” in *Proceedings of the 40th International Conference on Acoustics, Speech and Signal Processing (ICASSP 2015)*, Apr. 2015, pp. 708–712.
- [26] G. Montavon, W. Samek, and K.-R. Müller, “Methods for interpreting and understanding deep neural networks,” *Digital Signal Processing*, vol. 73, pp. 1–15, 2018.
- [27] S. Kolouri, S. R. Park, M. Thorpe, D. Slepcev, and G. K. Rohde, “Optimal mass transport: Signal processing and machine-learning applications,” *IEEE Signal Processing Magazine*, vol. 34, no. 4, pp. 43–59, July 2017.
- [28] R. Flamary, C. Févotte, N. Courty, and V. Emiya, “Optimal spectral transportation with application to music transcription,” in *Proceedings of the 29th International Conference on Neural Information Processing Systems*, ser. NIPS’16, Barcelona, Spain, Dec. 2016.
- [29] G. Hinton, O. Vinyals, and J. Dean, “Distilling the knowledge in a neural network,” in *Proceedings of the 28th International Conference on Neural Information Processing Systems, Workshop on Deep Learning and Representation Learning*, ser. NIPS’15, 2015.
- [30] D. Giannoulis, D. Barchiesi, A. Klapuri, and M. D. Plumbley, “On the disjointness of sources in music using different time-frequency representations,” in *Proceedings of the 2011 IEEE Workshop on Applications of Signal Processing to Audio and Acoustics (WASPAA 2011)*, Oct. 2011, pp. 261–264.
- [31] A. Liutkus, D. Fitzgerald, Z. Rafii, B. Pardo, and L. Daudet, “Kernel additive models for source separation,” *IEEE Transactions on Signal Processing*, vol. 62, no. 16, pp. 4298–4310, Aug 2014.
- [32] Y. Wang and D. Wang, “A deep neural network for time-domain signal reconstruction,” in *Proceedings of the 2015 IEEE International Conference on Acoustics, Speech and Signal Processing (ICASSP)*, April 2015, pp. 4390–4394.

- [33] G. Naithani, J. Nikunen, L. Bramsløw, and T. Virtanen, “Deep neural network based speech separation optimizing an objective estimator of intelligibility for low latency applications,” in *Proceedings of the 2018 IEEE International Workshop on Acoustic Signal Enhancement*, Sep. 2018.
- [34] W. K. Pratt, “Generalized Wiener filtering computation techniques,” *IEEE Transactions on Computers*, vol. C-21, no. 7, pp. 636–641, July 1972.
- [35] S. I. Mimilakis, E. Cano, D. Fitzgerald, K. Drossos, and G. Schuller, “Examining the perceptual effect of alternative objective functions for deep learning based music source separation,” in *Proceedings of the 52nd Asilomar Conference on Signals, Systems, and Computers*, 2018.
- [36] V. Papyan, Y. Romano, J. Sulam, and M. Elad, “Theoretical foundations of deep learning via sparse representations: A multilayer sparse model and its connection to convolutional neural networks,” *IEEE Signal Processing Magazine*, vol. 35, no. 4, pp. 72–89, July 2018.
- [37] R. Pascanu, G. Montufar, and Y. Bengio, “On the number of response regions of deep feedforward networks with piecewise linear activations,” in *Proceedings of the International Conference on Learning Representations (ICLR’14)*, 2014.
- [38] Z. Rafii, A. Liutkus, F. Stöter, S. I. Mimilakis, and R. Bittner, “The MUSDB18 corpus for music separation,” Dec 2017. [Online]. Available: <https://doi.org/10.5281/zenodo.1117372>
- [39] X. Glorot and Y. Bengio, “Understanding the difficulty of training deep feedforward neural networks,” in *Proceedings of the International Conference on Artificial Intelligence and Statistics (AISTATS’10)*, 2010, pp. 249–256.
- [40] D.-P. Kingma and J. Ba, “Adam: A method for stochastic optimization,” in *Proceedings of the International Conference on Learning Representations (ICLR-15)*, 2015.
- [41] P. Magron, R. Badeau, and A. Liutkus, “Lévy NMF for robust nonnegative source separation,” in *Proceedings of the 2017 IEEE Workshop on Applications of Signal Processing to Audio and Acoustics (WASPAA)*, Oct 2017, pp. 259–263.
- [42] J. Santos and T. Falk, “Investigating the effect of residual and highway connections in speech enhancement models,” in *Proceedings of the 32nd International Conference on Neural Information Processing Systems, Workshop on Interpretability and Robustness in Audio, Speech, and Language*, ser. NIPS’18, Montreal, Canada, Dec. 2018.
- [43] S. Dieleman and B. Schrauwen, “End-to-end learning for music audio,” in *Proceedings of the 39th International Conference on Acoustics, Speech and Signal Processing (ICASSP 2014)*, May 2014, pp. 6964–6968.